Title

AAVrh-10 transduces outer retinal cells in rodents and rabbits following intravitreal administration.

Journal

Gene Therapy, 26(9)

Authors

Zeng, Yong

Qian, Haohua

Wu, Zhijian

et al.

Publication Date

2019-09-01

DOI

10.1038/s41434-019-0094-3

Peer reviewed

HHS Public Access

Author manuscript

Gene Ther. Author manuscript; available in PMC 2024 September 11.

Published in final edited form as:

Gene Ther. 2019 September ; 26(9): 386–398. doi:10.1038/s41434-019-0094-3.

AAVrh-10 Transduces Outer Retinal Cells in Rodents and Rabbits Following Intravitreal Administration

Yong Zeng[1], **Haohua Qian**[2], **Zhijian Wu**[2], **Dario Marangoni**[1], **Paul Sieving**[1,2], **Ronald Bush**[1]

[1]Section on Translational Research for Retinal and Macular Degeneration, National Institute on Deafness and Other Communication Disorders, National Institutes of Health, Bethesda, Maryland, United States

[2]National Eye Institute, National Institutes of Health, Bethesda, Maryland, United States

Abstract

Recombinant adeno-associated virus (rAAV) has been widely used for gene delivery in animal models and successfully applied in clinical trials for treating inherited retinal disease. Although subretinal delivery of AAVs can effectively transduce photoreceptors and/or retinal pigmental epithelium (RPE), cells most affected by inherited retinal diseases, the procedure is invasive and complicated, and only delivers the gene to a limited retinal area. AAVs can also be delivered intravitreally to the retina, a much less invasive nonsurgical procedure. However, intravitreal administration of non-modified AAV serotypes tends to transduce only ganglion cells and inner nuclear layer cells. To date, most non-modified AAV serotypes that have been identified are incapable of efficiently transducing photoreceptors and/or RPE when delivered intravitreally. In this study, we investigate the retinal tropism of AAVrh10 vector administered by intravitreal injection to mouse, rat, and rabbit eyes. Our results demonstrate that AAVrh10 is capable of transducing not only inner retinal cells, but also outer retinal cells in all three species, though the transduction efficiency in rabbit was low. In addition, AAVrh10 preferentially transduced outer retinal cells in mouse models of retinal disease. Therefore, AAVrh10 vector could be a useful candidate to intravitreally deliver genes to photoreceptor and RPE cells.

Introduction

Inherited retinal diseases are a group of heterogenous disorders, most of which are caused by monogenic alterations resulting in degenerating photoreceptors and/or dysfunctional retinal pigment epithelium (RPE) that lead to impaired vision. Monogenic alterations can lead to either a lack of the normal protein resulting in functional insufficiency or to an abnormal protein producing a gain of toxic effect that damages retinal structure and/or interferes with retinal biophysiological function. Gene augmentation is being widely utilized to treat functional insufficiency in retinal disease or retard the progress of retinal degeneration [1-6]. Recombinant virus vectors that are replication deficient, including adenovirus, lentivirus,

Corresponding Author: Ronald A. Bush, National Institute on Deafness and Other Communication Disorders, National Institutes of Health, 50 South Drive, Rm 4339, MSC#8021, Bethesda, MD 20892-8021; bushr@nidcd.nih.gov.

Disclosure: Yong Zeng, None; Haohua Qian, None; Zhijian Wu, None; Dario Marangoni, None; Paul A. Sieving, None; Ronal A. Bush, None.

and adeno-associated virus (AAV), have been widely used as a vehicle to deliver the normal gene into diseased retinas and supplement functional protein in targeted cells [2, 6-9]. Among viral vectors, AAV is one of the most promising vehicles for therapeutic gene delivery because of its non-pathogenicity, low immunogenicity, long term therapeutic gene expression, broad range of host and cell type tropism, and the ability to transduce both dividing and non-dividing cells.

The retina is an ideal target for gene therapy because of its compartmentalization, easy accessibility, relatively immune-privileged status, and availability for noninvasive functional and structural examinations [10, 11]. Several clinical trials of gene therapy treatments for retinal diseases, including Leber congenital amaurosis [12], choroideremia [5], age-related macular degeneration [13], and X-linked retinoschisis (XLRS) [14, 15], have been conducted using an AAV-mediated delivery system. AAV2-mediated gene delivery has recently been approved by FDA to treat patients with hereditary retinal disease caused by biallelic *RPE65* mutations.

As most inherited retinal diseases affect photoreceptor and/or RPE cells, an effective treatment requires delivering vectors to transduce these outer retinal cells and induce expression of the normal gene in the targeted cells. There are two major routes of delivery to transduce cells in the outer retina: through the subretinal space or the vitreous cavity. Subretinal injection is widely used to deliver vector to produce high photoreceptor transduction with several serotypes of AAV, including AAV2, 5, 7, 8, and 9 [16-18], and the RPE can be effectively transduced by AAV1, 2, 4, 5, and 8 [17, 18]. However, subretinal injection requires specialized surgical skill, and the procedure itself induces retinal detachment between the photoreceptors and RPE which may cause permanent retinal damages such as central retinal thinning, macular hole formation and choroidal effusion [9, 19]. In addition, each subretinal injection can only deliver vector to a limited retinal area in a large eye. In contrast, intravitreal injection is much less invasive and has become a routine procedure performed in clinical outpatient practice for delivery of other drugs [20, 21]. A large study reported that the complication rate for intravitreal injection is less than 0.03% [22]. However, the main obstacle for using intravitreal injection to target outer retinal cells is the lack of AAV vectors capable of effectively transducing cells in the deep retinal layers, which include photoreceptors and RPE cells. Currently, the AAV2 serotype, which possesses a natural tropism for ganglion cells and inner retinal cells, is the most commonly used to deliver genes by intravitreal injection. AAV2-based capsid modifications, including by direct evolutionary screening and exposed surface amino-acid substitution, have been made to enhance its transduction profile [19, 23, 24]. In addition, AAV5, AAV8 and AAV9 variants have been generated for better retinal transduction by intravitreal injection through novel capsid design and amino-acid substitutions [25-28]. However, even though some of these modified vectors exhibit excellent transduction of outer retinal cells in mouse models [3, 19, 29], none of them is capable of achieving an efficient transduction in large animal models including non-human primates [30].

The needs for a serotype that can transduce outer retinal cells by intravitreal injection are growing rapidly. In addition, identifying new capsids with native tropism for photoreceptor/RPE cells via the vitreous will provide novel insights for modifications

and rational design to enhance vector infectivity or speed up the gene expression onset. AAVrh10 is a capsid isolated from rhesus monkey [31]. Due to its tropism for neurons, this vector has been used extensively as a carrier to deliver genes and treat central nervous system (CNS) diseases [32-35]. Giove et al reported in 2010 that AAVrh10 was capable of transducing ganglion cells, inner nuclear cells, Muller cells, and a few photoreceptor and RPE cells through intravitreal injection in mouse retina [36]. However, this vector has received little attention in the ophthalmology field. To investigate gene delivery capability of AAVrh10 and its retinal cellular tropism after intravitreal injection, we used a vector with enhanced green fluorescent protein (EGFP) driven by cytomegalovirus (CMV) promoter as a reporter gene, and examined retinal expression of fluorescent protein by fundus imaging and histology. We used a lower dose and longer incubation time than previously reported by Giove et al and included the eyes from three species: mouse, rat and rabbit.

Method and Material

Animals

Three lines of mice were used in these studies: *Rs1*-KO (generated previously in our lab [2]), which is the retinoschisin-null mouse model, *Rho*-KO (generated by Humphries et al [37]), which is the rod rhodopsin-null mouse model, and wildtype (littermates of *Rs1*-KO mouse). Rats (Sprague Dawley, SD), and rabbits (normal New Zealand White male) were also used. This research was conducted in accordance with the ARVO Statement on the Use of Animals in Ophthalmic and Vision Research and was approved by the Animal Care and Use Committee of the National Eye Institute. Mice were born and reared under 50-lux cyclic light (12 hour:12 hour) in the animal facility at NIH. Five to 6 weeks old rats were purchased from Taconic (Taconic, Derwood, MD, USA) and reared under standard animal room cyclic light (12 hour: 12 hour). Six to 8 months old rabbits were purchased from Covance (Covance, Princeton, NJ, USA) and reared under normal cyclic lighting (12 hour:12 hour). All animals were reared with food and water available ad libitum.

Intravitreal Injection

Recombinant AAVrh10-CMV-EGFP vector, which was packaged as described previously [38] in the core facility of NEI, was bilaterally administered by intravitreal injection into 4 *Rs1*-KO mice at age 5 to 5½ months, and 10 wildtype littermates at age 5 weeks to 6 months and 4 *Rho*-KO mice at postnatal day 3. AAVrh10-CMV-EGFP vector was bilaterally administered into six 6-week old SD rats. Mice and rats were anesthetized by intraperitoneal injection of ketamine (100 mg/kg) and xylazine (10 mg/kg), and one drop of 0.5% tetracaine topical anesthetic was applied to the cornea. One microliter of viral vector was injected into the adult WT and *Rs1*-KO mouse vitreous body and 0.3 microliter of viral vector was injected into 3-day old *Rho*-KO mouse vitreous body at a dose of 5×10^9 vector genomes (vg) /adult eye and 1.7×10^9 vg /baby eye. Five microliters of vector were injected into the rat vitreous cavity at three different doses: 2.5×10^9 vg/eye (n=4), 2.5×10^{10}vg/eye (n=4), and 2.5×10^{11} vg /eye (n=4). Injections were done through the sclera on the nasal side of the eye approximately 1 mm posterior to the limbus with a 10-μL Nanofil syringe with a removable 35-gauge needle (World Precision Instruments, Inc., Sarasota, FL, USA). AAvrh10-CMV-EGFP vector or saline was bilaterally administered into rabbit eyes. Rabbits

were anesthetized with IM ketamine (40 mg/kg) and xylazine (3 mg/kg) The eyelid margins and the conjunctiva at the injection site were disinfected by 5% povidone iodine in BSS. Fifty microliters of viral vector at two different doses, 2.8 x 10^{11}vg/eye (n=8) and 2.8 x 10^{12}vg/eye (n=4), or 50 microliters of saline (n=4) were injected into the vitreous cavity of each eye through the pars plana region in the superior temporal quadrant approximately 2 mm posterior to the limbus with a ½ cc insulin syringe with a permanently attached 28-gauge needle (ultrafine U-100 syringe-BD Biosciences, San Jose, CA). After injection, triple antibiotic ophthalmic ointment (neomycin, polymyxin B, and bacitracin) was applied to the eye.

Rabbit Fundus Imaging and Retina Sectioning

Fundus images were obtained using confocal scanning laser ophthalmoscopy (cSLO, Spectralis, Heidelberg Engineering, Franklin, MA) at 5 ½ weeks and 7 ½ weeks post injection for rabbits injected with 2.8 x 10^{12} vg/eye, and at 7 weeks and 11 weeks post injection for those injected with 2.8 x 10^{11} vg /eye. Rabbits were anesthetized with IM injection of ketamine and xylazine, their eyes dilated with topical administration of 1% tropicamide and 2.5 % phenylephrine, and the cornea lubricated with Systane Ultra. An eyelid speculum was inserted to keep the eye open during imaging. The fundi of rabbit eyes were viewed using a 55° wide-field lens in blue auto-fluorescence mode with a 488 nm laser to capture the high fluorescence region. Infrared reflectance and multi-color fundus images were also captured to document the fundus region and evaluate retinal conditions. Selected areas were further scanned and imaged with a 30° lens to provide better spatial resolution.

Two days after fundus image collection, rabbits were euthanized by anesthetic overdose at selected time points for evaluation of GFP expression. Prior to enucleation, each eye was marked for orientation using a suture of Vycril 5.0 in the temporal pole of the ocular bulb. After enucleation, the whole eye was immersed in 4% paraformaldehyde in PBS for 3 hours followed by removal of the anterior parts of the eye (lens, cornea and iris), the eye cup was fixed for an additional 16 hours. The tissue was then cryo-protected with a gradient of sucrose. Three days after incubation in the final concentration of 30% sucrose, the eyecup was embedded in Optimal Cutting Temperature (OCT). Cryosections (10 μm) were cut along the dorsal-ventral plane and collected beginning at the temporal (injection) margin of the eye. Two sections were taken every 100 μm up to the optic nerve and placed on the same slide. In the region of the optic nerve, two sections were taken every 40 μm. A total of 120 to 140 slides (240 to 280 sections) were made from each eye.

Rodent Fluorescent Eyecup Imaging and Retina Sectioning

Mice and rats were euthanized at 8 weeks post injection (PI) with CO_2 chamber, followed by cervical dislocation for mice and bilateral pneumothorax for rats. Eyeballs were enucleated with the third eyelid retained and fixed in 4% paraformaldehyde (PFA) in sodium phosphate buffer (PBS) on wet ice for 30 minutes, and then the cornea and lens were removed, and the eyecup fixed another 1.5 hours on wet ice. After washing three times with PBS, fluorescent images of the eyecups were obtained using a Nikon C2 fluorescence microscope (Nikon, Tokyo, Japan) with a 10x lens. All fluorescent eyecup images were centered on the brightest

fluorescent area or the optic nerve head (ONH) if entire eyecup was fluorescent to access the fluorescent intensity in each injected retina.

Eyecups were then placed in 30% sucrose in 1xPBS at 4°C overnight for cryopreservation followed by processing for cryosectioning. Approximately 30 sagittal sections of the injected eye were collected beginning at the nasal margin of the retina and proceeding through and including the ON head and approximately 200 μm of the temporal retina.

Fluorescent Intensity Measurement of Rat Eyecup

Fluorescent eyecup images were evaluated with ImageJ 1.48v (http://imagej.nih.gov/ij; provided in the public domain by the National Institutes of Health, Bethesda, MD, USA). They were first converted to back and white with the "Adjust Threshold" command, then the intensity threshold was adjusted to select areas positive for GFP fluorescence from background signals by comparison to the original images using the "Huang" method selected in the "threshold" window. Each fluorescent eyecup gave one measurement of the integrated density from the entire image, which is a sum of the number of pixels in the selected area with a brightness above the threshold, and this integrated density was used to assess the fluorescent level for each retina.

Analysis of the Distribution of Fluorescent cells and Identifying Transduced Inner Nuclear Cell Type

DAPI staining of section—Rabbit, rat and mouse retinal sections were dried at room temperature for 1 hour, and stained with 4′,6′-diamidino-2-phenylindole (DAPI; Invitrogen, Carlsbad, CA, USA) for 10 minutes, and washed with washing buffer for another 10 minutes followed by mounting with Fluorogel (Electron Microscopy Sciences, Hetfield, PA, USA). A Nikon C2 confocal microscope with Advanced Element software (Nikon, Tokyo, Japan) was used to capture and process retinal images, and image analysis was performed using image-editing software (Photoshop CS6; Adobe Systems, Inc., San Jose, CA, USA).

Immunofluorescence Assay—Rat and mouse retinal sections were rinsed in 0.1% Triton X-100 in PBS and preincubated with PBS containing 20% normal goat serum (Sigma, Steinheim, Germany) and 0.5% Triton X-100 at room temperature (RT) for 2 hours to permeabilize the tissue and block nonspecific antibody binding. Counter-staining to identify retinal cell types was conducted by incubating sections overnight at 4°C with a mixture of the primary antibodies listed in the Table 1 diluted in washing buffer. After washing with washing buffer, sections were incubated with an appropriate secondary antibody conjugated to red-fluorescent Alexa Fluor 568 dye or green-fluorescent Alexa Fluor 488 dye (Invitrogen, Carlsbad, CA, USA) for 1 hour at room temperature. The nuclei were stained with DAPI in washing buffer, and sections were mounted with Fluorogel. A Nikon C2 confocal microscope with Advance Element software (Nikon, Tokyo, Japan) was used to capture and process retinal images, and image analysis was performed by using image-editing software (Photoshop CS6; Adobe Systems, Inc.).

Results

Fundus Images

GFP fluorescence was detected in fundus images of rabbit eyes that received either 2.8 x 10^{12} vg/eye (n=4) or 2.8 x 10^{11} vg/eye (n=8) of AAVrh10-CMV-EGFP by intravitreal injection (Figure 1). At both 5 ½ (Figure 1b) and 7 ½ (Figure 1d) weeks post injection of 2.8 x 10^{12} vg/eye, GFP fluorescence was seen around the visual streak and in the inferior retina. Figure 1a and 1c are multicolor fundus images of the regions showing fluorescence in Figure 1b and 1d. These regions (red ovals) were further scrutinized using a 30° lens as shown in Figure 1b1, and 1d1 and 1d2 in which punctate GFP fluorescent dots are clearly visible. GFP fluorescent signals also form fine white lines (Figure 1b1, red arrow head), which resemble the optic nerve fibers. One eye that received 2.8 x 10^{11} vg/eye showed very strong fluorescence forming a bright white area along the retinal vasculature (Figure 1g) at 7 weeks PI, while the rest of the eyes at that dose had much less fluorescent signal at 7 weeks (Figure 1e and 1f) or 11 weeks PI (Figure 1h and 1i). The fluorescent white dots are distributed mostly along the retinal vasculature (Figure 1e to 1i, green arrow heads), just to the optic nerve head (Figure 1f and 1i, yellow arrow heads), in the area of the visual streak, and in the inferior retina (data not shown). The fluorescent signal intensity did not increase between PI time points for either dose, which indicates that AAVrh10 vector may reach peak expression by 5 to 6 weeks PI.

AAVrh10-CMV-EGFP vector was delivered by intravitreal injection into both eyes of six rats at three different doses, 2.5 x 10^{9} vg/eye (n=4), 2.5 x 10^{10} vg/eye (n=4) and 2.5 x 10^{11} vg/eye (n=4) in a volume of 5 ul. Representative fluorescent eyecups from each dose at 8 weeks PI are shown in figure 2A. Figure 2Aa and 2Ab are fluorescence fundus images of rat eyes receiving 2.5 x 10^{9} vg/eye and show a pattern of well separated green dots (Figure 2Aa and 2Ab, red arrow heads). Images from eyes that received 2.5 x 10^{10} vg per eye (Figure 2Ac and 2Ad) show more numerous fluorescent dots (red arrow heads) as well as lines of fluorescence (white arrows), and in some regions, broad areas of fluorescence (large white arrow head). Figure 2Ae and 2Af are representative fundus images from eyes receiving 2.5 x 10^{11} vg per eye that show more intense fluorescence spreading out to cover most of the retinal area and fluorescent green lines radiating out from the optic nerve head (white arrows). The retinal transduction efficiency, as measured by the density of fluorescence in fundus images, was improved significantly by increasing the vector dose (Figure 2B, nonparametric one-way ANOVA).

AAVrh10 vector was delivered via intravitreal injection into mouse eyes of three lines: Wildtype (n=20) and *Rs1*-KO (n=8) received 5 x 10^{9} vg per eye in a volume of 1μl, and *Rho*-KO mouse (n=8) received 1.7 x 10^{9} vg per eye in a volume of 0.3 ul. Eyecup fluorescent images were obtained at 8 weeks PI (Figure3). All twenty injected WT eyes showed GFP fluorescent signal, but there was large individual variation. Figure 3a-3d are four-representative fundus images of injected WT mice showing fluorescent signal limited to around the optic nerve head (Figure 3a) or covering larger areas including the entire retina (Figure 3d). The signal appears as scattered green dots (white arrow heads), green lines (white arrows), or broad areas of green (large yellow heads). Figure 3e-3h are

four-representative fluorescent eyecup images of injected *Rs1*-KO mice, and Figure 3i-3l are four-representative images of injected *Rho*-KO mice. The results of AAVrh10 vector injection in these two mouse models are similar to WT: fluorescent signal is present in all injected eyes, but with large individual variation. The distribution can be restricted to the optic nerve head area (Figure 3e and 3i) or encompass the entire retina (Figure 3h and 3l).

Retinal Cell Tropism of Intravitreal AAVrh10

Rabbit retina—GFP signal was detected in all injected rabbit eyes in sagittal cryosections of the retina taken from the nasal and temporal sides and through the optic nerve. As seen in fundus images, the degree of transgene expression varied across individuals. Figure 4 shows representative images of GFP fluorescence and DAPI staining in a cryosection from the retina shown in Figure 1b, which demonstrates the cellular tropism of AAVrh10 in rabbit retina based on cell shape and location. Figure 4a shows a region expressing relatively high fluorescent signal and the many types of retinal cells that are transduced by AAVrh10 vector, including ganglion cells (red arrow heads), horizontal cells (yellow arrow head), and Müller cells (white arrow heads). Figures 4b - 4e show images of a transduced horizontal cell (4b, yellow arrow head), Müller cells (4c, white arrow heads), ganglion cells and optic nerve fibers, and RPE cells, respectively (4d-4e, red arrow heads).

Since not many transduced cells exist in rabbit retinas, the cell morphology and localization are clearly defined on retinal sections without conducting the counter-staining study. We are able to recognize the transduced retinal cell type according to their morphology and localization. Therefore, the co-localization study using anti-GFP antibody and cell markers was not performed in rabbit retinal section.

Rat retina—Cryosections from rat eyecups were taken from regions that displayed green fluorescence and were stained with DAPI. Representative images are shown on figure 5. The distribution of green fluorescence can be categorized into three patterns: mainly targeting the inner retina (Figure 5Aa and 5Ab, ganglion cells: red arrow heads); mainly targeting the outer retina (5Ac and 5Ad, photoreceptors: white arrow heads; and RPE cells: red arrow heads); and targeting all retinal layers (5Ae and 5Af, from the GCL to the RPE cell layer, including INL and ONL with fluorescent process extend into IPL and OPL).

To identify the inner retinal cell types which are transduced by AAVrh10, the sections that show the highest GFP expression were selected for the counter-staining using anti-GFP antibody and cell markers. The antibodies that were used for immunofluorescent (IF) staining are listed in Table1. Figure 5Ba shows rod bipolar cells labelled with GFP/PKCα indicated by red arrow heads. Figure 5Bb shows GFP/calbindin labelled horizontal cells (red arrow heads), Figure 5Bc and 5Bd shows GFP/calretinin or GFP/parvalbumin labelled amacrine cells (red arrow heads), respectively. GFP positive ganglion cells are present in all panels of Figure 5B (white arrow heads). These results indicate that amacrine cells, horizontal cells, and rod bipolar cells are among the GFP positive cells in inner nuclear layer.

Mouse retina—The distribution of AAVrh10 transduced cells was analyzed in sagittal cryosections of mouse retina taken from regions showing fluorescence in fundus images of

mouse eyecups. DAPI staining was done to help determine retinal layers. Figure 6A shows four representative images of retinal sections from wildtype mouse, each with different GFP distributions. In Figure 6Aa, the transduced area is limited to just a few ganglion cells (red arrow heads). In other animals GFP positive cells are more widespread but are either predominantly in the inner retina (Figure 6Ab) or in photoreceptor cells (Figure 6Ac). 2 out of 20 injected eyes showed that the transduction occurred almost in the entire retina (Figure 6Ad), and all-layer-transduction happened in about 50% of the retinal area in these eyes. In another 4 injected eyes, the transduction occurred in more than 50% of the retina area, and 10% to 40% of the sections of these 4 eyes showed the all-layer-transduction. Müller cells are also GFP positive in some areas as shown in Figure 6Ab (white arrow head).

Unlike WT, most of GFP expression in *Rs1*-KO mouse is in photoreceptors and RPE cells with large variation in transduction efficiency. Transduction of outer retinal cells ranged from a few photoreceptor cells (Figure 6Ba), to most photoreceptor cells and RPE cells (Figure 6Bc), to almost all the photoreceptor cells and RPE cells (Figure 6Bd). Transduction efficiency varies greatly among the eyes, and is not correlated with the formation of cavities in *Rs*-KO mouse. For example, both retinal sections in either 6Ba and 6Bd showed no cavities, and yet transduction efficiency is much lower in figure 6Ba than in figure 6Bd. Likewise, both retinal sections in Figure 6Bc and in 6Bb have clear retinal cavities (white arrows), but the transduction efficiency is much higher in figure 6Bc than in 6Bb. These results suggest that retinal transduction efficiency of the outer retina by AAVrh10 is independent of the number and size of cavities.

Like in the *Rs1*-KO mouse, AAVrh10 transduced cells primarily in the outer retina of *Rho*-KO mouse (Figure 6C). Figure 6Ca shows an example in which the RPE only is transduced; figure 6Cb and 6Cc show examples of inner segment (IS) and a few photoreceptor cells in addition to RPE cells being transduced; figure 6Cd shows a retina in which all retinal layers are transduced.

To characterize the inner retinal cell types that are transduced by AAVrh10, sections that show the highest GFP expression were selected for counter-staining using cell markers and anti-GFP antibodies listed in Table 1. Figure 7A shows the counterstaining results of WT retina. The bottom panels are higher magnification images corresponding to the images in the top panel. In general, the number of transduced inner retinal cells is less in mouse retina than those observed in rat retina. There were no GFP/PKCα labelled bipolar cells detected as shown in figure 7Aa and 7Ae, but GFP/Calbindin labelled horizontal cells (Figure 7Ab and 7Af, white arrow head), GFP/calretinin labelled amacrine cells (Figure 7Ac and 7Ag, white arrow heads) and /or GFP/parvalbumin labelled amacrine cells (Figure 7Ah, white arrow head) were detected. The green fluorescent ganglion cells (Figure 7Ac yellow arrow heads) and the green fluorescent optic nerve fiber (Figure 7Ad, yellow arrow head) were detected as well. Figure 7B shows the counterstaining result of *Rs1*-KO mouse retina. Except for ganglion cells (Figure 7Bc and 7Bd, white arrow heads), we did not detect any GFP/PKCα positive bipolar cells, GFP/calbindin labelled horizontal cells, GFP/calretinin labelled amacrine cells, nor GFP/parvalbumin labelled horizontal cells or amacrine cells. Figure 7C shows the counterstaining result of *Rho*-KO mouse retina, the bottom panels are higher magnification images of the regions imaged in the top panel. Similar to WT

retina, there are calbindin positive horizontal cells (Figure 7Cb and 7Cf, white arrow heads), and calretinin positive (Figure 7Cc and 7Cg, white arrow heads) or parvalbumin positive amacrine cells (Figure 7Cd and 7Ch, white arrow heads) transduced by AAVrh10. The ganglion cells in some areas are transduced as well (Figure 7Cc, yellow arrow heads). No GFP positive rod bipolar cells were detected in this mouse model either.

Discussion

Our study demonstrated that intravitreal injections of AAVrh10 in mouse, rat, and rabbit eyes were capable of transducing not only in inner retina cells but also cells in the outer retina. Strongly transduced photoreceptor cells were detected in both rats and mice, but transduced rod bipolar cells were detected only in rats. In some area of retina, cells with Müller cell morphology and localization were transduced as well, though double labeling with a cell specific marker was not used. Transduced ganglion cells, horizontal cells, Müller cells, optic nerve fiber and RPE were detected in all three species, but the transduction efficiency was much lower in rabbit retina compared to rodent. The following are possible reasons for this: 1) difference in type of AAV receptors between the eyes of rodents and rabbit, 2) variation in the thickness and /or components of the inner limiting membrane (ILM) between the eyes of rodents and rabbit, 3) discrepancy in microenvironment of retinal cells between rodents and rabbit, and 4) difference in eye size which results in less physical damage and/or IOP (intraocular pressure) changes following intravitreal injection in rabbit than in rodent. Some of these same factors may be responsible for individual differences within species. Our study confirmed the findings of Giove et al [36] who found that AAVrh10 transduced GCL and INL cells in mice by 4 weeks after intravitreal injection. In addition, our study revealed that AAVrh10 can effectively transduce the photoreceptor layer and RPE in rodents and weakly transduce RPE in rabbits. The inconsistent findings between their study and ours may partially result from the difference in the length of incubation time after administering vector into the vitreous cavity. Instead of 4-weeks, we used an 8-week incubation time to allow the transgene to turn on, since it was reported that AAV2 vector may take up to 15 weeks to reach peak transduction after intravitreal injection [17, 39], and a self-complimentary AAV8 (scAAV8) vector took 6 to 8 weeks to reach its peak transduction (our unpublished data).

We found that the tropism of AAVrh10 vector in mouse models of retinal diseases was not exactly the same as in WT retina. In *Rs1*-KO and *Rho*-KO retinas, models of XLRS and RP, respectively, transduction was outer retina dominant in all injected eyes; transduced cells mostly resided in photoreceptors and RPE in these retinas. In WT, the distribution of transduce cells was either inner retina dominant, outer retina dominant or across all retinal layers. In another words, while the tropism in diseased retinas was consistently greater for the outer retina with some individual variation in transduction efficiency, the tropism of AAVrh10 in WT retina was more variable. It was previously reported that the transduction profile of AAV1,5,8 and 9 vectors delivered by intravitreal injection in a rat model of retina degeneration was different than in WT; there was increased transduction efficiency and altered tropism of AAV with viral particles reaching the photoreceptors and RPE rather than accumulating at the vitreoretina junction as they did in WT [40]. Thus, it will be more

meaningful to include disease related animal models in testing the retinal tropism of vector in preclinical studies of human retinal degenerative diseases.

We found that retinal transduction was unevenly distributed in all three species tested, but there was an especially large individual variation in mice, as we have observed in all of our preclinical studies of AAV gene therapy by intravitreal delivery [14]. Mice are widely used to study the tropism of AAV after intravitreal injection, and the availability of models of genetic retinal diseases is one reason for this. However, the mouse eye is small, and the space between the limbus and the retina is very narrow; the injecting needle must pass through retinal tissue to deliver from in the intravitreous. So, the mouse retina is very easily injured when performing intravitreal injection. The injured retina can introduce DNA damage and DNA repair. It's been known for decades that DNA damage and repair in targeted tissue can enhance AAV transduction efficiency [41, 42]. In addition to physical contact by the needle insertion causing injury, intraocular pressure elevation due to the rapid increase in vitreal volume (20% in mouse) could stress the retina and subsequently may change the cellular microenvironment. For instance, the elevation of intraocular pressure can cause a change in the distribution of optic nerve dynein protein [43]. Dynein is required for transporting cellular cargoes, including endosomes, toward the microtubule minus ends [44]. Trafficking of endosome containing AAV particles from the cellular membrane toward the nuclear membrane along the microtubule is a crucial step for the onset of AAV-mediated transgene expression [45] . Cells from different individuals or even different cells in the same region don't necessarily enter into the same cell cycle in response to stress [46]. Thus, the impact of injury or intraocular pressure elevation varies from individual to individual and region to region in a given retina, possibly resulting in variable transduction efficacy. The large individual variation in AAV transduction in mouse that we and others have found [47, 48] may be partly the result of differing stress-induced changes in the microenvironment which plays a key role in the AAV transduction profile.

Although results presented in this study illustrated AAVrh10 as a promising vector for transducing outer retina cells by intravitreal delivery, modifications to its capsid might further increase its effectiveness for treating retinal diseases. Some retinal diseases, for example certain mutations in the RPE65 gene in patients with Leber Congenital Amaurosis (LCA) [49] and certain mutations of the rhodopsin gene in patients with retinitis pigmentosa (RP) [50], can cause very rapid retinal degeneration, which requires fast onset of the transgene. Both self-complementary AAV (scAAV) vector and AAV capsid variants demonstrated a faster onset of transgene and a higher level of expression than conventional non-modified single strand AAV vector [19, 23, 50]. scAAV vector bypasses the rate-limiting step of second-strand DNA synthesis [51]; surface amino-acid substitution prevents proteasome-mediated degradation of viral particles [52]; and novel capsids enhance entry of AAV particles into the cell subsequently improving vector infectivity [26]. Reid et al. obtained a significantly higher proportion of retina transduced by using a chimeric AAV2 vector, in which the combination of tyrosine mutation and 7m8 insertion was employed in its capsid [48]. Making these modifications to the AAVrh10 capsid, which we have shown is already more effective at transducing outer retinal cells through intravitreal administration than other wild type AAV vectors, may give the AAVrh10 vector higher transduction efficiency, faster transgene onset and novel tropism compared to other modified

AAV serotypes. Moreover, a self-complementary transgene genome could be used with these mutant capsids to further enhance transduction efficiency if the size of transgene fits into the capacity of an AAV vector. Since the neutralizing-antibody seroprevalences are only 21% for AAVrh10 compared to 71% for AAV2 [53], and preexisting neutralizing antibodies can compromise the effective gene transfer [54], AAVrh10 may be a better candidate for treating retinal disease by intravitreal injection. In addition to improving AAV vector infectivity by capsid modification, an effort should also be made to increase the susceptibility of targeted cells to AAV infection by changing the cellular microenvironment without permanently damaging the structure and function of the targeted cells.

Acknowledgement

The authors wish to thank Dr. James M. Wilson (University of Pennsylvania, Philadelphia, Pennsylvania) for providing the AAVrh10 capsid DNA construct, Suja Hiriyanna for producing the AAVrh10-CMV-EGFP vector, Maria Santos and Jinbo Li for technical assistance, and Wei Li, Wenhan Yu for reviewing the manuscript. The research was supported by the Intramural Research Program of the National Institutes of Health, National Institute on Deafness and other Communication Disorders and the National Eye Institute.

References

1. Acland GM, Aguirre GD, Ray J, Zhang Q, Aleman TS, Cideciyan AV et al. Gene therapy restores vision in a canine model of childhood blindness. Nature genetics 2001; 28(1): 92–5. [PubMed: 11326284]
2. Zeng Y, Takada Y, Kjellstrom S, Hiriyanna K, Tanikawa A, Wawrousek E et al. RS-1 Gene Delivery to an Adult Rs1h Knockout Mouse Model Restores ERG b-Wave with Reversal of the Electronegative Waveform of X-Linked Retinoschisis. Investigative ophthalmology & visual science 2004; 45(9): 3279–85. [PubMed: 15326152]
3. Byrne LC, Dalkara D, Luna G, Fisher SK, Clerin E, Sahel JA et al. Viral-mediated RdCVF and RdCVFL expression protects cone and rod photoreceptors in retinal degeneration. The Journal of clinical investigation 2015; 125(1): 105–16. [PubMed: 25415434]
4. Du W, Tao Y, Deng WT, Zhu P, Li J, Dai X et al. Vitreal delivery of AAV vectored Cnga3 restores cone function in CNGA3−/−/Nrl−/− mice, an all-cone model of CNGA3 achromatopsia. Human molecular genetics 2015; 24(13): 3699–707. [PubMed: 25855802]
5. MacLaren RE, Groppe M, Barnard AR, Cottriall CL, Tolmachova T, Seymour L et al. Retinal gene therapy in patients with choroideremia: initial findings from a phase 1/2 clinical trial. Lancet 2014; 383(9923): 1129–37. [PubMed: 24439297]
6. Han Z, Conley SM, Naash MI. Gene therapy for Stargardt disease associated with ABCA4 gene. Advances in experimental medicine and biology 2014; 801: 719–24. [PubMed: 24664763]
7. Cashman SM, Gracias J, Adhi M, Kumar-Singh R. Adenovirus-mediated delivery of Factor H attenuates complement C3 induced pathology in the murine retina: a potential gene therapy for age-related macular degeneration. The journal of gene medicine 2015; 17(10–12): 229–43. [PubMed: 26369397]
8. Matet A, Kostic C, Bemelmans AP, Moulin A, Rosolen SG, Martin S et al. Evaluation of tolerance to lentiviral LV-RPE65 gene therapy vector after subretinal delivery in non-human primates. Translational research : the journal of laboratory and clinical medicine 2017; 188: 40–57 e4. [PubMed: 28754419]
9. Jacobson SG, Cideciyan AV, Ratnakaram R, Heon E, Schwartz SB, Roman AJ et al. Gene therapy for leber congenital amaurosis caused by RPE65 mutations: safety and efficacy in 15 children and adults followed up to 3 years. Archives of ophthalmology 2012; 130(1): 9–24. [PubMed: 21911650]
10. Bennett J, Chung DC, Maguire A. Gene delivery to the retina: from mouse to man. Methods in enzymology 2012; 507: 255–74. [PubMed: 22365778]
11. Takahashi K, Igarashi T, Miyake K, Kobayashi M, Yaguchi C, Iijima O et al. Improved Intravitreal AAV-Mediated Inner Retinal Gene Transduction after Surgical Internal Limiting Membrane

Peeling in Cynomolgus Monkeys. Molecular therapy : the journal of the American Society of Gene Therapy 2017; 25(1): 296–302. [PubMed: 28129123]

12. Maguire AM, Simonelli F, Pierce EA, Pugh EN Jr., Mingozzi F, Bennicelli J et al. Safety and efficacy of gene transfer for Leber's congenital amaurosis. The New England journal of medicine 2008; 358(21): 2240–8. [PubMed: 18441370]
13. Rakoczy EP, Lai CM, Magno AL, Wikstrom ME, French MA, Pierce CM et al. Gene therapy with recombinant adeno-associated vectors for neovascular age-related macular degeneration: 1 year follow-up of a phase 1 randomised clinical trial. Lancet 2015; 386(10011): 2395–403. [PubMed: 26431823]
14. Bush RA, Zeng Y, Colosi P, Kjellstrom S, Hiriyanna S, Vijayasarathy C et al. Preclinical Dose-Escalation Study of Intravitreal AAV-RS1 Gene Therapy in a Mouse Model of X-linked Retinoschisis: Dose-Dependent Expression and Improved Retinal Structure and Function. Human gene therapy 2016; 27(5): 376–89. [PubMed: 27036983]
15. Cukras C, Wiley HE, Jeffrey BG, Sen HN, Turriff A, Zeng Y et al. Retinal AAV8-RS1 Gene Therapy for X-Linked Retinoschisis: Initial Findings from a Phase I/IIa Trial by Intravitreal Delivery. Molecular therapy : the journal of the American Society of Gene Therapy 2018; 26(9): 2282–2294. [PubMed: 30196853]
16. Allocca M, Mussolino C, Garcia-Hoyos M, Sanges D, Iodice C, Petrillo M et al. Novel adeno-associated virus serotypes efficiently transduce murine photoreceptors. Journal of virology 2007; 81(20): 11372–80. [PubMed: 17699581]
17. Auricchio A, Kobinger G, Anand V, Hildinger M, O'Connor E, Maguire AM et al. Exchange of surface proteins impacts on viral vector cellular specificity and transduction characteristics: the retina as a model. Human molecular genetics 2001; 10(26): 3075–81. [PubMed: 11751689]
18. Natkunarajah M, Trittibach P, McIntosh J, Duran Y, Barker SE, Smith AJ et al. Assessment of ocular transduction using single-stranded and self-complementary recombinant adeno-associated virus serotype 2/8. Gene therapy 2008; 15(6): 463–7. [PubMed: 18004402]
19. Dalkara D, Byrne LC, Klimczak RR, Visel M, Yin L, Merigan WH et al. In vivo-directed evolution of a new adeno-associated virus for therapeutic outer retinal gene delivery from the vitreous. Science translational medicine 2013; 5(189): 189ra76.
20. Solomon SD, Lindsley K, Vedula SS, Krzystolik MG, Hawkins BS. Anti-vascular endothelial growth factor for neovascular age-related macular degeneration. The Cochrane database of systematic reviews 2014; (8): CD005139. [PubMed: 25170575]
21. Jain P, Sheth J, Anantharaman G, Gopalakrishnan M. Real-world evidence of safety profile of intravitreal bevacizumab (Avastin) in an Indian scenario. Indian journal of ophthalmology 2017; 65(7): 596–602. [PubMed: 28724817]
22. Englander M, Chen TC, Paschalis EI, Miller JW, Kim IK. Intravitreal injections at the Massachusetts Eye and Ear Infirmary: analysis of treatment indications and postinjection endophthalmitis rates. The British journal of ophthalmology 2013; 97(4): 460–5. [PubMed: 23390167]
23. Mowat FM, Gornik KR, Dinculescu A, Boye SL, Hauswirth WW, Petersen-Jones SM et al. Tyrosine capsid-mutant AAV vectors for gene delivery to the canine retina from a subretinal or intravitreal approach. Gene therapy 2014; 21(1): 96–105. [PubMed: 24225638]
24. Petrs-Silva H, Dinculescu A, Li Q, Min SH, Chiodo V, Pang JJ et al. High-efficiency transduction of the mouse retina by tyrosine-mutant AAV serotype vectors. Molecular therapy : the journal of the American Society of Gene Therapy 2009; 17(3): 463–71. [PubMed: 19066593]
25. Dalkara D, Byrne LC, Lee T, Hoffmann NV, Schaffer DV, Flannery JG. Enhanced gene delivery to the neonatal retina through systemic administration of tyrosine-mutated AAV9. Gene therapy 2012; 19(2): 176–81. [PubMed: 22011645]
26. Khabou H, Desrosiers M, Winckler C, Fouquet S, Auregan G, Bemelmans AP et al. Insight into the mechanisms of enhanced retinal transduction by the engineered AAV2 capsid variant −7m8. Biotechnology and bioengineering 2016; 113(12): 2712–2724. [PubMed: 27259396]
27. Khabou H, Garita-Hernandez M, Chaffiol A, Reichman S, Jaillard C, Brazhnikova E et al. Noninvasive gene delivery to foveal cones for vision restoration. JCI insight 2018; 3(2).

28. Kay CN, Ryals RC, Aslanidi GV, Min SH, Ruan Q, Sun J et al. Targeting photoreceptors via intravitreal delivery using novel, capsid-mutated AAV vectors. PloS one 2013; 8(4): e62097. [PubMed: 23637972]
29. Byrne LC, Ozturk BE, Lee T, Fortuny C, Visel M, Dalkara D et al. Retinoschisin gene therapy in photoreceptors, Muller glia or all retinal cells in the Rs1h−/− mouse. Gene therapy 2014; 21(6): 585–92. [PubMed: 24694538]
30. Ramachandran PS, Lee V, Wei Z, Song JY, Casal G, Cronin T et al. Evaluation of Dose and Safety of AAV7m8 and AAV8BP2 in the Non-Human Primate Retina. Human gene therapy 2017; 28(2): 154–167. [PubMed: 27750461]
31. Gao G, Alvira MR, Somanathan S, Lu Y, Vandenberghe LH, Rux JJ et al. Adeno-associated viruses undergo substantial evolution in primates during natural infections. Proceedings of the National Academy of Sciences of the United States of America 2003; 100(10): 6081–6. [PubMed: 12716974]
32. Hordeaux J, Dubreil L, Deniaud J, Iacobelli F, Moreau S, Ledevin M et al. Efficient central nervous system AAVrh10-mediated intrathecal gene transfer in adult and neonate rats. Gene therapy 2015; 22(4): 316–24. [PubMed: 25588740]
33. Winner LK, Beard H, Hassiotis S, Lau AA, Luck AJ, Hopwood JJ et al. A Preclinical Study Evaluating AAVrh10-Based Gene Therapy for Sanfilippo Syndrome. Human gene therapy 2016; 27(5): 363–75. [PubMed: 26975339]
34. Sondhi D, Johnson L, Purpura K, Monette S, Souweidane MM, Kaplitt MG et al. Long-term expression and safety of administration of AAVrh.10hCLN2 to the brain of rats and nonhuman primates for the treatment of late infantile neuronal ceroid lipofuscinosis. Human gene therapy methods 2012; 23(5): 324–35. [PubMed: 23131032]
35. Mondo E, Moser R, Gao G, Mueller C, Sena-Esteves M, Sapp E et al. Selective Neuronal Uptake and Distribution of AAVrh8, AAV9, and AAVrh10 in Sheep After Intra-Striatal Administration. Journal of Huntington's disease 2018.
36. Giove TJ, Sena-Esteves M, Eldred WD. Transduction of the inner mouse retina using AAVrh8 and AAVrh10 via intravitreal injection. Experimental eye research 2010; 91(5): 652–9. [PubMed: 20723541]
37. Humphries MM, Rancourt D, Farrar GJ, Kenna P, Hazel M, Bush RA et al. Retinopathy induced in mice by targeted disruption of the rhodopsin gene. Nature genetics 1997; 15(2): 216–9. [PubMed: 9020854]
38. Auricchio A, Hildinger M, O'Connor E, Gao GP, Wilson JM. Isolation of highly infectious and pure adeno-associated virus type 2 vectors with a single-step gravity-flow column. Human gene therapy 2001; 12(1): 71–6. [PubMed: 11177544]
39. Yang GS, Schmidt M, Yan Z, Lindbloom JD, Harding TC, Donahue BA et al. Virus-mediated transduction of murine retina with adeno-associated virus: effects of viral capsid and genome size. Journal of virology 2002; 76(15): 7651–60. [PubMed: 12097579]
40. Kolstad KD, Dalkara D, Guerin K, Visel M, Hoffmann N, Schaffer DV et al. Changes in adeno-associated virus-mediated gene delivery in retinal degeneration. Human gene therapy 2010; 21(5): 571–8. [PubMed: 20021232]
41. Russell DW, Alexander IE, Miller AD. DNA synthesis and topoisomerase inhibitors increase transduction by adeno-associated virus vectors. Proceedings of the National Academy of Sciences of the United States of America 1995; 92(12): 5719–23. [PubMed: 7777575]
42. Alexander IE, Russell DW, Miller AD. DNA-damaging agents greatly increase the transduction of nondividing cells by adeno-associated virus vectors. Journal of virology 1994; 68(12): 8282–7. [PubMed: 7966621]
43. Martin KR, Quigley HA, Valenta D, Kielczewski J, Pease ME. Optic nerve dynein motor protein distribution changes with intraocular pressure elevation in a rat model of glaucoma. Experimental eye research 2006; 83(2): 255–62. [PubMed: 16546168]
44. Xiang X, Qiu R, Yao X, Arst HN Jr., Penalva MA, Zhang J. Cytoplasmic dynein and early endosome transport. Cellular and molecular life sciences : CMLS 2015; 72(17): 3267–80. [PubMed: 26001903]

45. Xiao PJ, Samulski RJ. Cytoplasmic trafficking, endosomal escape, and perinuclear accumulation of adeno-associated virus type 2 particles are facilitated by microtubule network. Journal of virology 2012; 86(19): 10462–73. [PubMed: 22811523]

46. Roesch K, Stadler MB, Cepko CL. Gene expression changes within Muller glial cells in retinitis pigmentosa. Molecular vision 2012; 18: 1197–214. [PubMed: 22665967]

47. Da Costa R, Roger C, Segelken J, Barben M, Grimm C, Neidhardt J. A Novel Method Combining Vitreous Aspiration and Intravitreal AAV2/8 Injection Results in Retina-Wide Transduction in Adult Mice. Investigative ophthalmology & visual science 2016; 57(13): 5326–5334. [PubMed: 27784063]

48. Reid CA, Ertel KJ, Lipinski DM. Improvement of Photoreceptor Targeting via Intravitreal Delivery in Mouse and Human Retina Using Combinatory rAAV2 Capsid Mutant Vectors. Investigative ophthalmology & visual science 2017; 58(14): 6429–6439. [PubMed: 29260200]

49. Morimura H, Fishman GA, Grover SA, Fulton AB, Berson EL, Dryja TP. Mutations in the RPE65 gene in patients with autosomal recessive retinitis pigmentosa or leber congenital amaurosis. Proceedings of the National Academy of Sciences of the United States of America 1998; 95(6): 3088–93. [PubMed: 9501220]

50. Sarra GM, Stephens C, Schlichtenbrede FC, Bainbridge JW, Thrasher AJ, Luthert PJ et al. Kinetics of transgene expression in mouse retina following sub-retinal injection of recombinant adeno-associated virus. Vision research 2002; 42(4): 541–9. [PubMed: 11853771]

51. McCarty DM, Monahan PE, Samulski RJ. Self-complementary recombinant adeno-associated virus (scAAV) vectors promote efficient transduction independently of DNA synthesis. Gene therapy 2001; 8(16): 1248–54. [PubMed: 11509958]

52. Zhong L, Li B, Jayandharan G, Mah CS, Govindasamy L, Agbandje-McKenna M et al. Tyrosine-phosphorylation of AAV2 vectors and its consequences on viral intracellular trafficking and transgene expression. Virology 2008; 381(2): 194–202. [PubMed: 18834608]

53. Thwaite R, Pages G, Chillon M, Bosch A. AAVrh.10 immunogenicity in mice and humans. Relevance of antibody cross-reactivity in human gene therapy. Gene therapy 2015; 22(2): 196–201. [PubMed: 25410741]

54. Calcedo R, Vandenberghe LH, Gao G, Lin J, Wilson JM. Worldwide epidemiology of neutralizing antibodies to adeno-associated viruses. The Journal of infectious diseases 2009; 199(3): 381–90. [PubMed: 19133809]

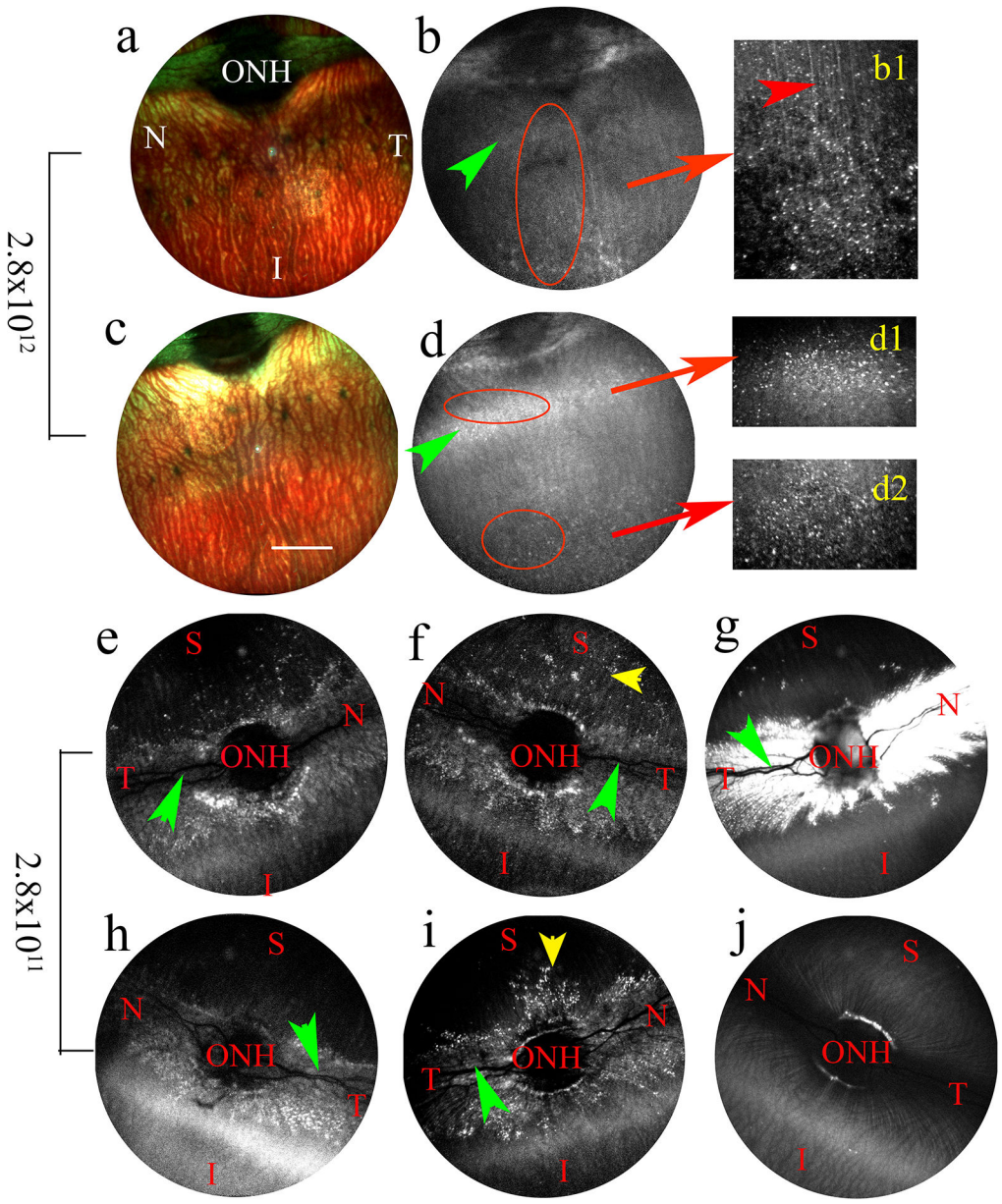

Figure 1.

Representative fundus images of rabbit eyes injected with two different doses of AAVrh10-CMV-EGFP, 2.8 x 10^{12} (a-d) and 2.8 x 10^{11} (e-i). (a-b) The multi-color and GFP fluorescence fundus images obtained from one rabbit eye injected with 2.8 x 10^{12} vg/eye and collected at 5 ½ weeks PI. (c-d) The multi-color and fluorescence images for another rabbit eye collected at 7 ½ weeks. Images were captured with a 55° wide-field lens, and green arrow heads in 1b and 1d point to the visual streak. (b1, d1, d2) The fluorescent signal representing transgene expression in the regions highlighted with red ovals in (b and d) images obtained with a 30° lens. Fluorescent retinal cells appear as punctate white dots, and optic nerve fibers as white lines (b1, red arrow head). Figures e -g are fluorescent fundus images of rabbit eyes injected with 2.8 x 10^{11} vg/eye obtained at 7 weeks PI, and

(h) and (i) were obtained at 11 weeks PI. A representative fundus image obtained at 11 weeks PI from an eye injected with saline is shown in (j). Green arrow heads point to the retinal vasculature, and yellow arrow heads point to fluorescent cells. N, nasal; I, inferior; T, temporal; ONH, optic nerve head. *Scale bar* for figure 1a - 1j: 3000 μm.

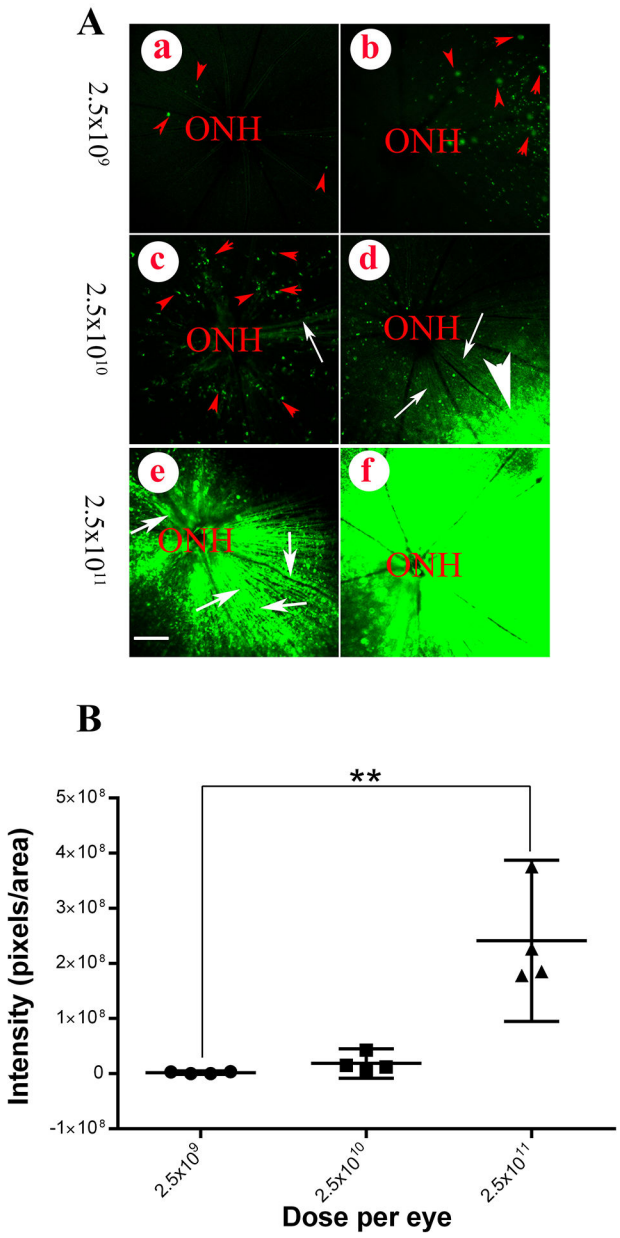

Figure 2.

GFP fluorescence in rat retinas eight weeks PI of three different doses of AAVrh10-CMV-EGFP. (A) Representative fluorescent images of rat eyecups receiving 2.5 x 10^9 vg/eye (a and b), 2.5 x 10^{10} vg/eye (c and d), and 2.5 x 10^{11} vg/eye (e and f). Red arrow heads point to fluorescent cells, white arrows point to fluorescent optic fiber and large white arrow head points to fluorescent retinal area. (B) The fluorescence intensity represented by integrated density as measured with Image J (see Methods) from eyes receiving each of the three doses of AAVrh10-CMV-EGFP. The fluorescence intensity produced by 2.5 x 10^{11} vg/eye was significantly higher than with 2.5 x 10^9 vg/eye (one-way ANOVA, nonparametric test), indicating a dose-dependent trend. ONH, optic nerve head. *Scale bar*: 200 μm.

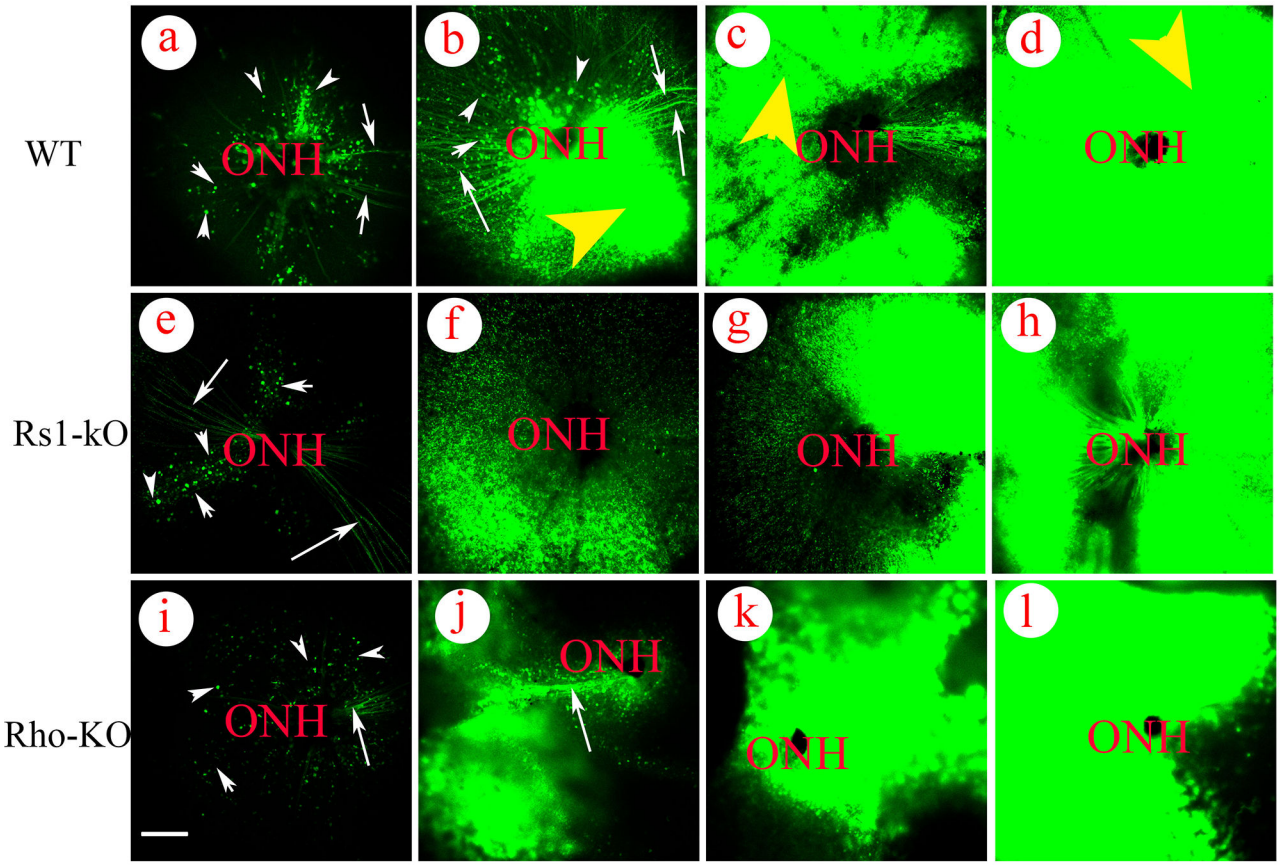

Figure 3.

GFP fluorescence in mouse retina eight weeks following intravitreal injection of AAVrh10-CMV-EGFP. Representative fluorescent images of eyecups from WT mice receiving 5 x 10^9 vg/eye (a-d), *Rs1*-KO mice receiving 5 x 10^9 vg/eye (e-h), and *Rho*-KO mice receiving 1.7 x 10^9 vg/eye (i-l). White arrow heads point to green fluorescent cells, white arrows point to fluorescent optic nerve fibers, and large yellow arrow heads point to fluorescent retinal area. ONH, optic nerve head. *Scale bar*: 200 μm.

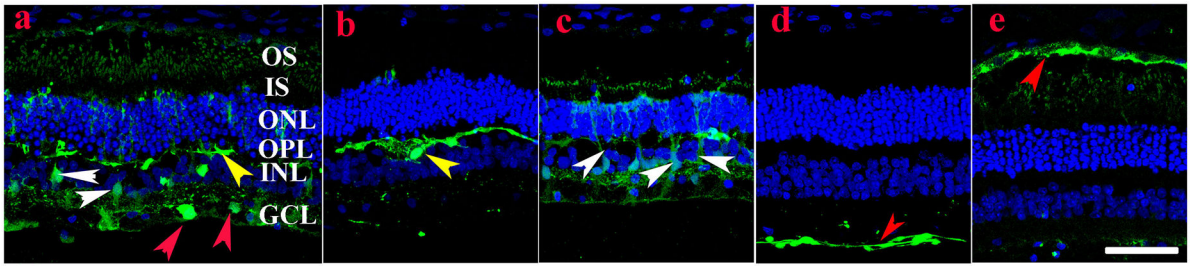

Figure 4.

Cellular tropism of AAVrh10 in rabbit retina receiving 2.8 x 10^{12} vg/eye. (a) Transduced cells in the GCL layer (red arrow heads), horizontal cell (yellow arrow head), and Müller cells (white arrow heads). (b) Transduced horizontal cell (yellow arrow head), (c) Müller cells (white arrow heads), (d) ganglion layer (red arrow head), and (e) RPE cells (red arrow head). Sections were stained with DAPI (blue) to show the nuclear layers. GCL, ganglion cell layer; OS, outer segment; IS, inner segment; ONL, outer nuclear layer; OPL, outer plexiform layer; INL, inner nuclear layer. *Scale bar*: 50 μm.

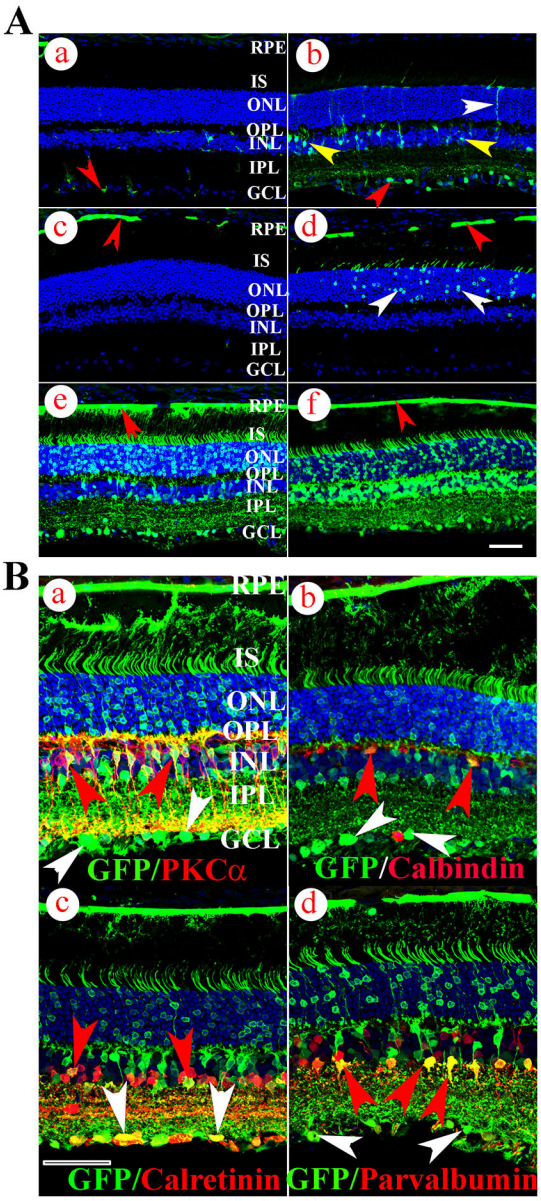

Figure 5.

Cellular tropism of AAVrh10 in the rat retinas receiving 2.5 x 10^{10} vg/eye (Aa, Ac and Ad) and 2.5 x 10^{11} vg/eye (Ab, Ae, Af and B). (A) GFP fluorescence in sagittal cross sections that represent different transduction efficiencies. Sections were stained with DAPI (blue) to show the nuclear layers. In some retinas, AAVrh10 predominantly transduced cells in the inner retina (a and b), including the GCL (red arrow heads) and INL (yellow arrow heads), and a few Müller cells (white arrow) spanning the inner and outer layers. In other retinas, outer retinal cell transduction was dominant (c, d), including RPE cells (red arrow heads) and photoreceptor cells (white arrow heads). Figures e and f show retinas in which cells in all layers were transduced, including the GCL, INL, and ONL, inner segments, and RPE cells. (B) identifies inner retinal cell types stained with GFP antibody using counter-staining with cell specific markers: (a) PKCα positive bipolar cells (red arrow heads); (b) calbindin

positive horizontal cells (red arrow heads); (c) calretinin positive amacrine cells (red arrow heads) and (d) parvalbumin positive amacrine cells (red arrow heads). White arrow heads point to fluorescent ganglion cells (a – d). RPE, retinal pigmental epithelium cells; IS, inner segment; ONL, outer nuclear layer; OPL, outer plexiform layer; INL, inner nuclear layer; IPL, inner plexiform layer; GCL, ganglion cell layer. *Scale bar* (Af and Bc): 50 μm.

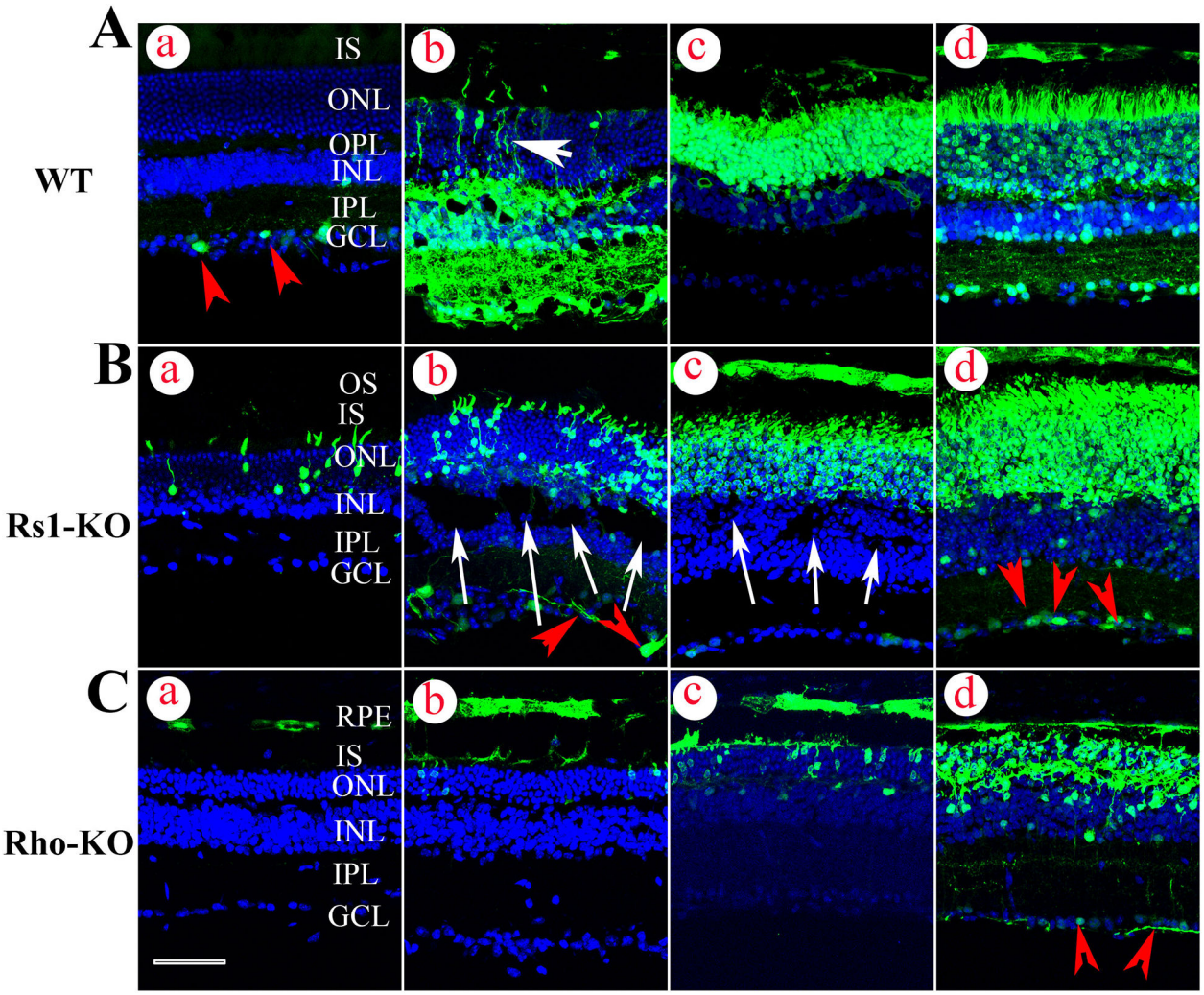

Figure 6.

Retinal transduction profiles of AAVrh10-GFP in three different mouse strains following intravitreal administration of 5 x 10^9 vg/eye (A and B) and 1.7 x 10^9 vg/eye (C). Sagittal cross sections of retinas from 4 different mice show the range of transduction profile in each strain. Sections were stained with DAPI (blue) to show the nuclear layers. (A) WT: ganglion cell only (a, red arrow heads); inner retinal cell dominant (b); outer retinal cell dominant (c); and all retinal layers (d) including GCL, INL, ONL, IS, RPE, and a few Müller cells in some areas (b, white arrow head). (B) *Rs1*-KO and (C) *Rho*-KO transduced mouse retinas. In these two diseased retina mouse models, AAVrh10 transduced outer retinal with various efficiencies: a few photoreceptor cells (Ba) and RPE cells (Ca); more than half of the photoreceptor cells (Bc) and RPE cells (Bc and Cc); most of the photoreceptor cells and RPE cells (Bd and Cd). Green fluorescent ganglion cells and optic nerve fiber are detected in some area as well (Bb, Bd, and Cd, red arrow heads). White arrows point to the cavities in *Rs1*-KO (Bb and Bc). GCL, ganglion cell layer; OS, outer segment; IS, inner segment; ONL, outer nuclear layer; OPL, outer plexiform layer; INL, inner nuclear layer. *Scale bar*: 50 μm.

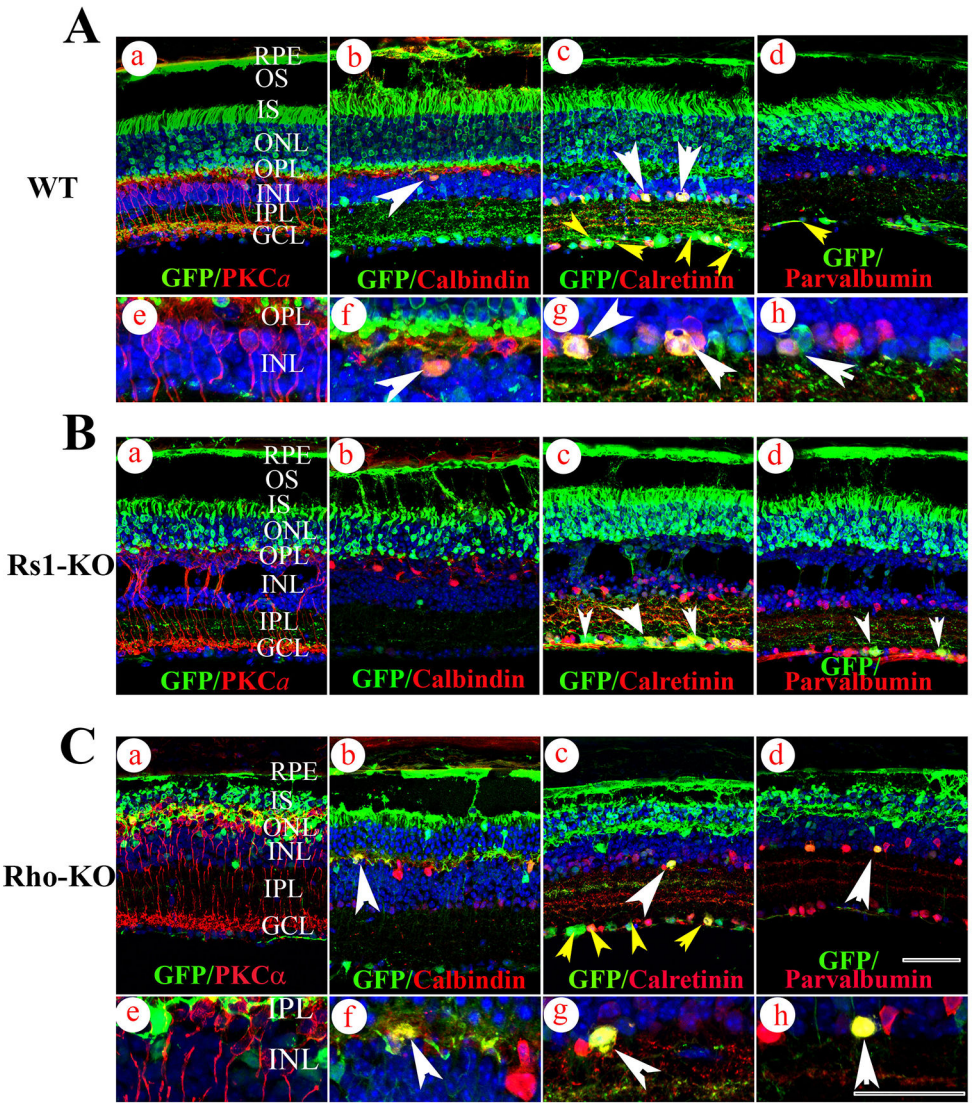

Figure 7.

Identification of inner retinal cell types in WT (A), *Rs1*-KO (B), and *Rho*-KO (C) mouse retinas after intravitreal injection of AAVrh10-GFP at 5 x 10^9 vg/eye (A and B) and 1.7 x 10^9 vg/eye (C). Retinas were counter-stained with GFP antibody and specific cell markers, and the lower panels in (A) and (C) show a higher magnification of the images in the corresponding upper panel. (A) WT mouse retina. (a and e): PKC*a* counter-staining shows no clearly doubled labeled rod-bipolar cells. (b and f): calbindin positive horizontal cells (white arrow heads). (c and g): calretinin positive amacrine cells (white arrow heads) and ganglion cells (small yellow arrow heads). (d and h) parvalbumin positive amacrine cell (white arrow head). (B) *Rs1*-KO mouse retina. There were no GFP positive inner retinal cells that could be counterstained with PKCα (a), calbindin (b), calretinin (c), or parvalbumin (d). White arrow heads indicate calretinin or parvalbumin positive ganglion cells (c and d). (C) *Rho*-KO mouse retina. (a and e): PKC*a* counter-staining shows no clearly doubled labeled rod-bipolar cells. (b and f): calbindin positive horizontal cells (white arrow heads). (c and g): calretinin positive amacrine cells (white arrow heads), and ganglion

cells (small yellow heads). (d and h): parvalbumin positive amacrine cells (white arrow heads). GCL, ganglion cell layer; OS, outer segment; IS, inner segment; ONL, outer nuclear layer; OPL, outer plexiform layer; INL, inner nuclear layer. *Scale bar* (Cd and Ch): 50 μm.

Table 1

List of Primary Antibodies Used in Immunohistochemistry

Name	Target	Host	Dilution	Product Source
GFP	GFP	Rabbit	1:1,000	TP401, Torrey Pines, Biolabs Inc., Biolabs Inc., Secaucus, NJ
		Mouse	1:1,000	2272, Cell Signaling Technology Inc., Danvers, MA 01923
Calbindin	Horizontal cell	Mouse	1:2,000	C9848, Sigma-Aldrich Inc., Louis, MO USA
Calretinin	Amacrine cell Ganglion cell	Rabbit	1:5,000	AB5045, Millipore Corporation, Bedford, MA USA
PKCα	Bipolar cell	Mouse	1:500	sc-8393, Santa Cruz Biotechnology Inc., Dallas, TX USA
Parvalbumin	Horizontal cell Amacrine cell Ganglion cell	Rabbit	1:1,000	Ab11427, Abcam Inc., Cambridge, MA USA